Experimental characterization of diffusive-thermal instabilities in CO_2-diluted H_2-CH_4-CO unstrained diffusion flames

Elie Antar[*,a], Julien Delavande[a] and Etienne Robert[a]

[a]Department of Mechanical Engineering, Polytechnique Montréal, Montréal, Québec, H3T 1J4, Canada

Abstract

The combustion of multi-fuel mixtures is experimentally studied for the first time in unstrained diffusion flames, where the parasitic hydrodynamic effects present in common research burners are negligible. A broad range of H_2-CO-CH_4 fuels highly diluted in CO_2 is investigated to provide an understanding of the intrinsic diffusive-thermal instabilities (DTIs) that onset in low calorific biomass-derived syngas. For each fuel blend, the burning intensity or the Damköhler number (D_a) is gradually reduced, going through the marginal stability state where DTIs first appear, down to the lean extinction limit. Flame stability limits are provided. From the large difference between the Lewis numbers of the multiple fuel species (Le_i), the cells that onset due to H_2 are seen to interact and compete with the pulsations from CO and CH_4, leading to superimposed cellular-pulsating instabilities. These are thoroughly characterized by measuring the pulsations amplitude, frequency, cell size, number of cells, and fraction of the flame sheet actively burning. An effective fuel Lewis number ($Le_{F,eff}$) calculated from the fuel mixture composition is introduced and used along with the Damköhler number to map the DTIs observed. At lower $Le_{F,eff}$ and D_a, the cellular attributes of the superimposed instabilities dominate, while at larger Lewis numbers and the near marginal stability state, pulsations prevail.

Keywords: Unstrained; Diffusion flame; Diffusive-thermal instabilities; Syngas

1. Introduction

Combustion instabilities are critical phenomena that can damage combustion systems as well as contribute to detrimental effects such as local extinction, pressure fluctuations, and incomplete combustion [1]. Instabilities can arise from the flame interacting with the system/combustion chamber, ex: thermoacoustic instabilities [2], or they can be intrinsic and pertain to the combustion process itself, ex: diffusive-thermal instabilities (DTIs) [3]. The focus of this work is DTIs, which

[*] Corresponding author Email: elie.antar@polymtl.ca

are for instance, relevant in low-emissions lean burners. DTIs can result in cellular [4] or pulsating flame fronts [5]. They are well known to occur in both premixed and non-premixed configurations. In the latter, since diffusive-thermal effects mainly control the complex extinction and re-ignition processes, hydrodynamic effects can be eliminated from the stability analysis as they play a secondary role [6]. This significant simplification has stimulated the development of numerous stability models based on the unstrained one-dimensional diffusion flame theoretical construct [7], where fundamental insight into DTIs in single-fuel mixtures has been gained, as discussed below. We experimentally replicate this idealized configuration here to investigate DTIs in multi-fuel mixtures.

As shown in Figure 1, the combustion chamber of the idealized one-dimensional chambered diffusion flame is a straight duct that is supplied at the bottom with fuel at a constant velocity via a semi-permeable membrane, and is exposed to constant conditions at the top. These are assumed to be maintained by a sufficiently fast stream flowing across the top boundary, uniformly removing the combustion products and supplying the counter-diffusing oxidizer. An analytical solution for the steady case can be readily derived since only one coordinate is required to describe the structure of the planar flames. This has been previously discussed in detail elsewhere [8].

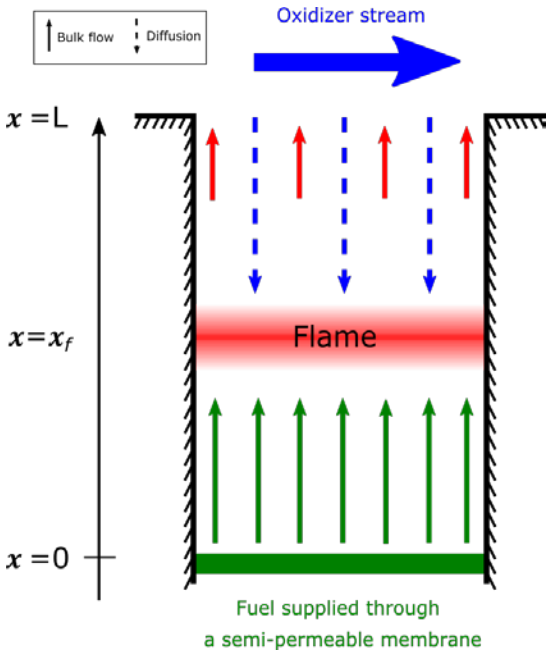

Figure 1: Schematic representation of the idealized one-dimensional chambered diffusion flame theoretical construct.

The steady solutions constitute the basic state of stability models that introduce perturbations in planar flames and monitor their response over time [9–11]. These models predict stability when operating far from extinction, and the possibility of DTIs depending on different physical parameters when the lean extinction limit is approached. The theoretical work by Metzener and Matalon [12] is one of the most exhaustive studies to date, where a broad range of parameters was investigated for single-fuel mixtures, such as distinct non-unity Lewis numbers for the fuel (Le_F) along with the oxidizer (Le_o), mixture strength, and flow conditions. It was shown that when DTIs develop in diffusion flames, the reaction sheet exhibits excess or deficiency in available enthalpy ($h_f \neq 0$). This is driven by differential and preferential diffusion of mass or heat (non-unity and unequal Lewis numbers) occurring at Damköhler numbers (D_a) smaller than that of the marginal stability state (D_a^*). The Damköhler number is the ratio of the characteristic diffusion time over chemical reaction time. At $D_a < D_a^*$, cells generally form at Lewis numbers sufficiently below unity, and pulsations onset at high Lewis numbers.

An experimental realization of essentially unstrained one-dimensional diffusion flames was introduced by Robert and Monkewitz [13]. The same burner is used in the present work, in which hydrodynamic effects are avoided by evenly supplying the counter-diffusing reactant and removing the combustion products along the same axis, as discussed in detail in section 2.1. Flow field measurements [13] revealed that the stable flames generated by this burner are subject to minimal residual stretch on the order of $0.05 s^{-1}$, and that their temperature along with species concentration profiles are in close agreement with the idealized analytical solution. The maximum temperature agrees within 50˚C with the adiabatic flame temperature (T_a), demonstrating minimal heat loss effects, especially when operating near the extinction limit where DTIs are observed. Consequently, this burner has been used [14] to validate the DTIs scaling laws predicted by stability theories in single-fuel flames for the first time uncoupled from hydrodynamic effects. The important role played by the Lewis numbers in controlling the instability type was confirmed, as H_2-CO_2 flames with Le_{H_2} = 0.25 produced cellular flames, while CH_4-CO_2 mixtures with $Le_{CH_4} =$ 0.82 yielded planar intensity pulsations. Nonetheless, the nature of DTIs formed in multi-fuel mixtures of these distinct combustible gases remains unknown.

The case of H_2-CH_4-CO fuel mixtures diluted in CO_2 is treated in this paper. These mixtures are representative of dry biomass-derived syngas [15], where the combined presence of H_2, with

high diffusivity, and CO/CH_4 with much lower mobility implies that the instability patterns and scaling laws are difficult to predict. The importance of efficiently burning these highly-diluted mixtures on the overall energy balance of biorefineries is significant, particularly for small-scale decentralized implementations [16], well suited to the distributed nature of biomass resources. Previous studies on the stability of syngas flames are largely based on premixed configurations, such as spherically expanding flames [17,18], flat flame McKenna burners [19,20], and Bunsen flames [21,22]. Aspects such as flammability limits, flame structure, and flame speed have been treated. However, the instabilities observed in the burners used were significantly driven by hydrodynamic effects, and were mainly cellular with no reference to any simultaneous flame front oscillations that may onset from CH_4 or CO species.

The goal of this paper is to experimentally investigate the stability of unstrained syngas diffusion flames, where fundamental insight into intrinsic diffusive-thermal phenomena can be obtained in conditions with negligible hydrodynamic and buoyancy disturbances. Starting from the Burke–Schumann limit, where the Damköhler number is very large, extinction is approached for each fuel mixture by decreasing Da to the marginal stability state, until DTIs are observed, and then to extinction. The parameter space of mixture composition is mapped, with the type of DTIs reported along with their characteristics, such as cell size, pulsating amplitude, and frequency. A generalized DTIs map for syngas mixtures is derived at the end, in terms of a fuel mixture effective Lewis number and the Damköhler number.

2. Methodology

2.1. Experimental facility

Figure 2 shows the experimental configuration of the one-dimensional unstrained diffusion flame burner [23] used in this study. The cross section of the combustion chamber is 77.5 × 77.5 mm with a geometric length of $L_{geom} = 40$ mm. For a uniform reactants supply, the burner features two arrays of 31 × 31 hypodermic needles with OD: 1.0 mm and ID: 0.8 mm, placed on a 2.5 mm Cartesian grid at both ends of the combustion chamber. To ensure that temperature, velocity, and species gradients are sufficiently reduced and flame flatness is maximized, a 1 mm thick quartz cylinder with a 45 mm outer diameter is wedged between both needles array in the combustion chamber, as shown in inset c) of Figure 2, with the measurements performed in the inner flame.

The desired H_2, CH_4, CO, and CO_2 fuel mixture composition is introduced into the burner through the bottom needle array using Hastings model HFC-202 flow controllers. The bulk flow rate is kept fixed at 7 SLPM, resulting in an upward fuel velocity of U = 19.42 mm/s at the bottom of the burner, where gas is approximately at standard conditions of temperature and pressure. To denote the fuel mixtures, the relative molar fraction of H_2 to CO ($X_{H_2,CO}$), the relative amount of CH_4 to the two other combustible species (X_{CH_4}), and the total fuel concentration (X_F) are used. The oxidizer stream, comprised of 100% O_2, is supplied uniformly through the top needles array at flow rates between 3.5 and 10 SLPM, and reaches the reaction zone only through one-dimensional counter-diffusion against the flow of combustion products, as shown schematically in Figure 2 b). The products are evacuated through another array of 32 × 32 curved stainless steel tubes (OD:1.4 mm and ID:1.2 mm) that are interlaced in the oxidizer injection array (Figure 2 a), and the outlet of which is exposed to atmospheric pressure, which is marginally lower than the pressure inside the combustion chamber. Heaters and thermocouples are fitted within the two reactants injection and exhaust plenums to control the temperature of the combustion zone boundaries and avoid condensation within the exhaust stream.

The nature of the oxidant supply in the burner implies the existence of a thin layer just below the top needles, as shown in inset b) of Figure 2. Here, PIV measurements [13] have shown that the flow is locally three-dimensional and that a portion of the supplied oxidizing species is directly evacuated upwards with the combustion products. Below this so-called injection layer, which has a thickness (Δ) that was conservatively measured to be below 3.0 mm using laser Doppler anemometry (LDA) [23], species concentration becomes highly uniform across the combustion chamber and their transport becomes one-dimensional, mimicking the idealized chambered diffusion flame configuration, with lateral variations in mixture strength below 10% across the flame width, as confirmed by mass spectrometer measurements [13,23]. Therefore, the effective length of the one-dimensional unstrained combustion zone is $L = L_{geom} - \Delta = 40 - 3 = 37$ mm.

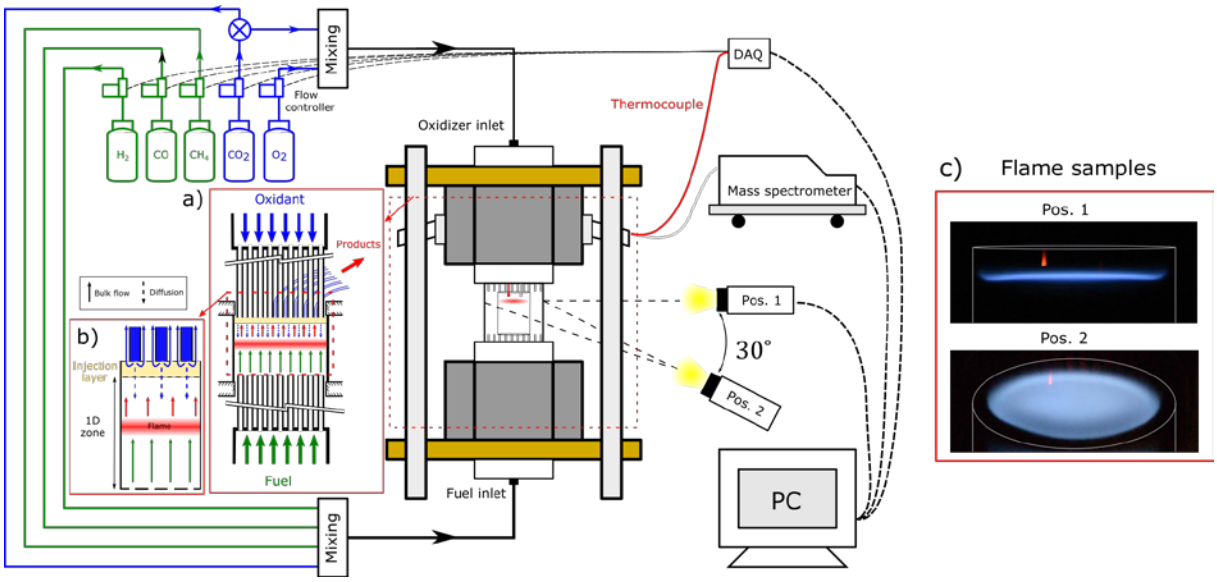

Figure 2: Schematic representation of the experimental facility used to create one-dimensional unstrained diffusion flames. Cross-sectional views of the burner showing a) the injection and exhaust needles, and b) the injection layer and the dimensional combustion zone. c) Flame images captured from positions 1 and 2.

2.2. Diagnostics

Due to the aforementioned injection layer, the species concentrations at the top of the one-dimensional combustion zone cannot be directly determined from the mixture properties of the injected oxidant stream. A thoroughly calibrated mass spectrometer [24] is used, where gas samples are collected 3.0 mm below the injection needles, and analyzed in real-time to obtain the concentration of the major species O_2, CO_2, and H_2O, with a relative accuracy of 5%. These measurements are used to evaluate the mixture strength (ϕ), which is defined as the ratio of the fuel to oxygen mass fractions at the boundaries of the one-dimensional combustion zone, normalized by their stoichiometric proportions [25].

The thermophysical properties of the reactants and flames produced are evaluated by applying the experimentally measured boundary conditions in a one-dimensional chambered diffusion flame model implemented in Matlab using the Cantera software package [26]. The Lewis numbers are evaluated at the flame location using the multicomponent transport properties model described in Kee et al. [27]. Excellent agreement between flame structures obtained using this numerical approach and experiments on stable planar diffusion flames has been previously reported [13]. In addition, agreement in terms of flame position can be seen from Figure 3, which presents the simulated syngas flame structure along with the spatial variation of the sampled light intensity

from the experiments. Distance is made non-dimensional using the length of the one-dimensional combustion region, $L = 37$ mm. The fuel species mass fractions (Y_F) are normalized with their concentration at the fuel inlet ($Y_{F,0}$), and finally the oxygen mass fraction (Y_O) is scaled with its concentration at the top of the domain and mixture strength ($Y_{O,L}\phi$).

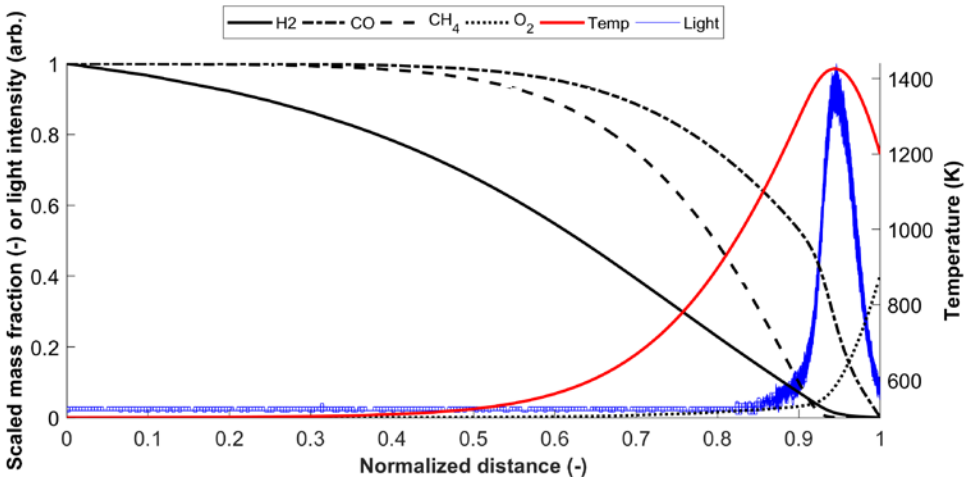

Figure 3: Flame structure from the idealized one-dimensional diffusion flame model, and experimentally measured light intensity signal for a mixture with $X_{H_2,CO}$ = 75%, X_{CH_4} = 15%, X_F = 30%, and ϕ = 2.5.

The flame location in the burner is determined by analysing images acquired using a digital still camera (Nikon D750) placed perpendicularly to the burner axis, shown as position 1 in Figure 2. To minimize imprecisions from acquired noise, a sampling window that spans 50% of the flat flame width is taken, in which the average location of the maximum light intensity from each pixel column is determined. This optically measured flame position with a spatial resolution of 0.047 mm/pixel or 0.12% discretization uncertainty was previously verified [13] to coincide with the maximum temperature, as also shown in Figure 3, and minimum reactants concentration. The maximum emitted light intensity is also used as a proxy for the flame chemical reaction rate. Its temporal variation is sampled at a rate of 30 Hz, and the Fourier transform is computed to determine the frequency and amplitude of the pulsations.

When spatial inhomogeneity in excessively cellular flames prevents the reliable determination of the emitted light intensity, the variation in flame position (x_f) is used to characterize the intensity of pulsations. As an example, comparisons between the flame position and maximum light intensity signal obtained as the pulsating instability develops are shown in Figure 4, for two planar flames with CH_4-CO fuel fractions of 75-25% and 45-55%. It can be seen that the

frequencies of both the position and light intensity signals are equal, and that their amplitude of oscillations is proportional to each other. The slight phase delay that is observed as the flame position trails the intensity variation, confirms that the pulsating DTI is intrinsically a variation in the reaction rate, with the flame position then adapting to the change in energy release. These observations are particularly evident with CH_4-CO 45-55%, as the pulsations intensity grows, but they were reflected in all measurements taken.

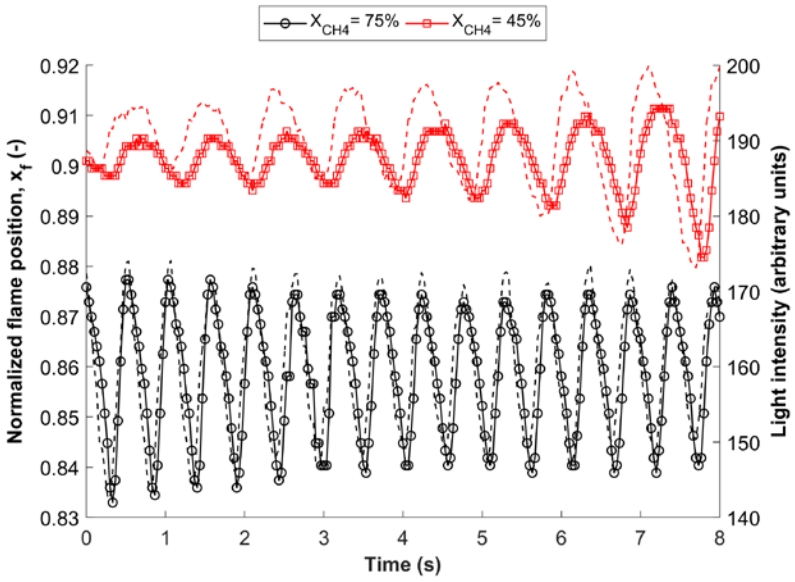

Figure 4: Temporal variation of flame position (—), and maximum light intensity emitted (---) for two pulsating CH_4-CO flames with X_{CH_4} = 75%, X_F = 17.5%, ϕ = 0.90, and X_{CH_4} = 45%, X_F = 16.5%, ϕ = 0.84.

To capture cellular instabilities, another camera is used to view the flame from below, with a 30˚ upward angle (position 2, Figure 2). An image analysis code implemented in Matlab is used to compute the fraction of the cylinder cross-section where the flame burns, as well as the number and distance between the cells that form on the periphery of the combustion zone. For the latter, the light intensity signal along a circle that is centered in the middle of the flame and that passes through each of the outermost cells is extracted, as shown in Figure 5. The mean arc length between each peak is computed and represents the reported cell size in this study.

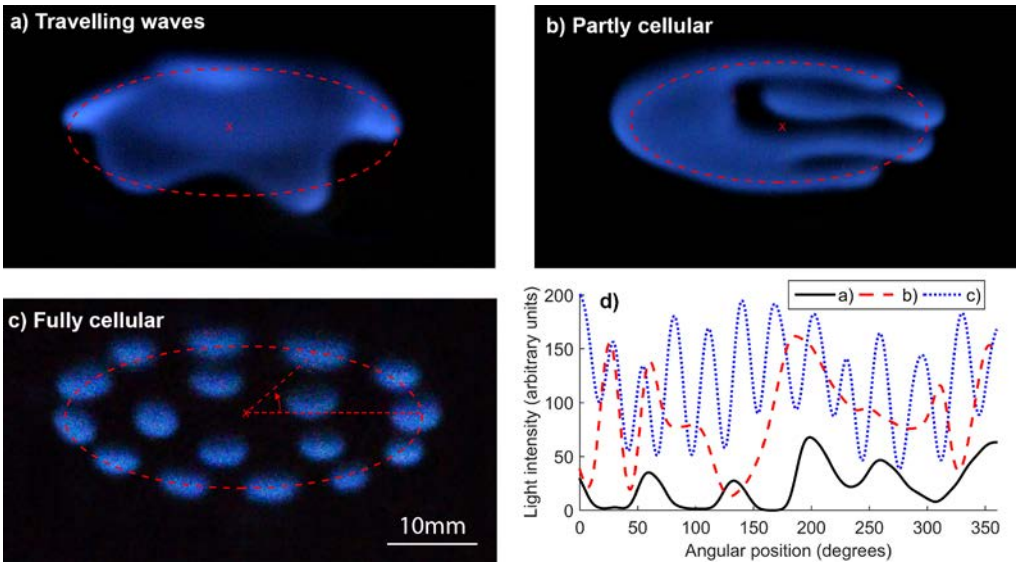

Figure 5: a) Flame with travelling waves at $X_{H_2,CO}$ = 75%, X_F = 22%, and ϕ = 0.49, b) partly cellular flame at X_{H_2CO} = 75%, X_F = 19%, ϕ = 0.63, and c) fully cellular flame at X_{H_2CO} = 100%, X_F = 17%, and ϕ = 0.75, with X_{CH_4} always 0%. d) Gaussian-filtered light intensity along circles that pass through the centers of the outermost cells for each of the three cellular flames shown, used to calculate cell size.

2.3. Parameters of interest

Theoretically, the onset and characteristics of DTIs in one-dimensional unstrained diffusion flames are dependant on the following five parameters [12]: $\Delta T, D_a, \phi, Le_F,$ and Le_o. In this section, the methods used to control these parameters in our experimental configuration are discussed. The first parameter, ΔT, is the temperature difference between the top (T_L) and bottom boundaries of the one-dimensional combustion zone. Its influence on the general behaviour of DTIs is relatively minor, and it is kept approximately constant in our burner at $\Delta T = 700^{\circ}$C using the plenum heaters.

The second parameter, D_a, can be varied through the flame temperature, which we adjust using the fuel CO_2 dilution. The computation of D_a from the experiments is discussed latter in section 3.1. It should be noted that in theoretical studies, D_a is controlled through the residence time by changing the bulk velocity, while keeping other parameters constant. However, in the experimental configuration used, the range of achievable bulk velocities does not cause significant changes in D_a, and the strong coupling between the bulk velocity and the flow in the injection layer, which alters the top boundary conditions, further complicates this approach.

The third parameter, the mixture strength, is measured using the mass spectrometer described in the previous section. For a given fuel concentration, the mixture strength can be varied by adjusting the flow rate or O_2 concentration of the supplied oxidizer stream into the burner. However, the operational ϕ range over which the one-dimensional nature of the flame is preserved can be limited by the appearance of convective instabilities. As ϕ largely controls the flame position, leaner flames position themselves lower in the burner. Consequently, the hot gas layer associated with the flame heat release is lowered in the relatively cooler surrounding fluid, and the temperature stratification becomes unstable leading to Rayleigh–Bernard convection cells [28]. These undesirable buoyancy-driven effects are easy to detect and avoid, since they lead to very large-amplitude cells or ridges that always grow unsustainably with time, and cause the flame to collapse on the bottom needles array of the burner. Consequently, the onset of Rayleigh–Bernard convection cells are averted by studying only sufficiently high flames with $x_f \geq 0.8$.

The forth parameter affecting DTIs is the fuel Lewis number Le_F, which is species-specific for the commonly considered case of single-fuel mixtures. However, in the current study involving multi-fuel mixtures, the simultaneous presence of more than one combustible species naturally motivates the adoption of a fuel mixture effective Lewis number $Le_{F,eff}$:

$$Le_{F,eff} = X_{H_2} Le_{H_2} + X_{CO} Le_{CO} + X_{CH_4} Le_{CH_4} \quad (1)$$

with X_i being the molar fraction of species i relative to the other the combustible species in the supplied fuel stream. The Lewis numbers of each reactant in Eq. 1 are computed using the one-dimensional chambered diffusion flame model supplied with the experimentally-measured boundary conditions as discussed in section 2.2. These Lewis numbers are largely determined by the nature of the most abundant species, which is always CO_2 for the low caloric value syngas mixtures considered here [16]. Therefore, these and the Lewis number of the oxidizer (fifth parameter affecting DTIs) do not vary significantly upon changing the fuel composition. As shown in section 3.1, Le_{H_2} only varies from 0.23-0.28, Le_{CH_4} from 0.81-0.96, and Le_{CO} from 0.89-1.07, and finally Le_o from 0.88-1.06 with an average value of 0.97 for all the flame discussed in this paper. The fuel composition is nevertheless reflected in $Le_{F,eff}$, through the X_i terms (Eq. 1), whereby a broad fuel composition range such that $Le_{H_2} \leq Le_{F,eff} < Le_{CO}$ is investigated.

For every $Le_{F,eff}$, we transition from a strongly burning stable flame operating near the Burke-Schumann limit ($D_a \rightarrow \infty$) towards the marginal stability state where the first instabilities are observed. This is accomplished by reducing the fuel concentration at the lower ϕ limit of the burner such that no buoyancy-driven instabilities arise. To maximize the mapped instabilities beyond the marginal stability state, ϕ is gradually varied by changing the oxidizer flow rate within its operation range for every decrement in X_F, until dilution-induced extinction is attained. Only weakly-burning lean flames are investigated, which are relevant to low-emissions syngas combustion. Weakly-burning rich flames are not considered since such conditions cannot be achieved in the experimental configuration used, as the required large ϕ values would push the flame outside the one-dimensional combustion domain and into the injection layer ($x_f > 1$).

3. Results

3.1. H_2-CO_2 mixtures

The instability type caused by each of the three fuel species (H_2/CO/CH_4) is first individually studied by considering simple fuel mixtures. Starting with H_2-CO_2 mixtures, with $Le_{F,eff} = Le_{H_2}$ being approximately 0.25, the flame stability limits are presented in Figure 6. DTIs are observed within the shaded zone, while the hatched region represents conditions that could not be tested in our burner as the instabilities are not sustainable, or since buoyancy-driven instabilities appear at low mixture strengths. The latter can be readily identified from the dramatically large and three-dimensional convective cells, which are an order of magnitude larger than the stationary cells from DTIs. This behaviour of buoyancy-driven instabilities was confirmed using a broad range of fuel mixtures, including single-fuel CH_4, where unlike cells from DTIs, buoyancy-driven convection cells of invariable size was always observed, when the flame was sufficiently low. A comparison between Rayleigh–Bernard convection cells, and diffusive-thermal cells is shown in supplementary Figure 1 and Figure 2. In the former, the inner quartz cylinder is removed from the combustion chamber to better illustrate the instability size.

Travelling waves are the first DTI pattern observed at $X_F = 23.5\%$, as represented by pentagram symbols with filled circular centers in Figure 6. They consist of five large amplitude waves/cells rotating around the flame center at frequencies between 3.45 and 3.6 revolutions per second (Figure 5 a). Rotating cells were previously reported on several occasions in H_2 diffusion

flames, such as the experimental work by: Lo Jacono et al. [6] using an axisymmetric jet burner, and Hu et al. [29] along with Shopoff et al. [30] using opposed-flow tubular burners. As can be seen from Figure 6, travelling waves are the only instabilities observed down to $X_F = 21.5\%$. Beyond this point, rotation stops, holes in the center of the flame start to appear for the first time, and the flame turns partly cellular (Figure 5 b) as indicated by the circular symbols with open stars in Figure 6. At $X_F = 18\%$ full cellularity (Figure 5 c) is finally attained, whereby 17 stationary and completely detached cells form.

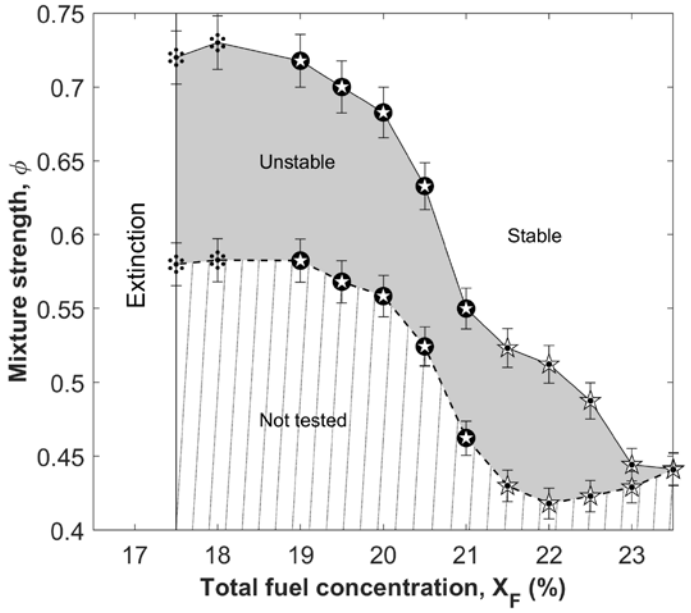

Figure 6: Flame stability limits in terms of the fuel concentration and mixture strength for H_2-CO_2 mixtures. The instability type is represented by symbols. (✯): Travelling waves, (✪): partly cellular, and (✣): fully cellular. The error bars indicate the uncertainty from the mass spectrometer measurements.

The increase in cellularity at lower X_F, or in other words, lower D_a, is consistent with previous theoretical predictions on the stability of unstrained diffusion flames [31], as shown in the stability map of Figure 7. At higher D_a, H_2 flames are located outside the stationary cells zone, whereby mixed instability modes such as travelling waves or oscillatory cells are predicted [12]. By reducing D_a, the Lewis number range that leads to stationary cells increases, and eventually includes the H_2 flames observed in our burner. To further illustrate this, the Damköhler numbers of the unstable flames are estimated as per the following definition [31]:

$$D_a = (\lambda/\rho_a c_p U^2)(R^0 T_a/E)^3(\nu_x c_p \overline{W}/qR^0 W_f)\mathfrak{B}Y_{f,o}p_0 \exp(-E/RT_a) \quad (2)$$

Owing to the lack of suitable empirical data, the values of the activation energy E and the Arrhenius pre-exponential factor $\mathfrak{B}$ are assumed constant for a given fuel. They are selected such that Damköhler number at the marginal stability state for a given $Le_{F,eff}$ is equal to unity [14]. This means that the D_a calculated in this paper is a relative one, for a given fuel composition. This yields an approximation of the top branch of the typical S-shaped response curve of diffusion flames shown in Figure 8, where the observed transition from travelling waves to full cellularity at lower Da is highlighted for unstable H_2 flames.

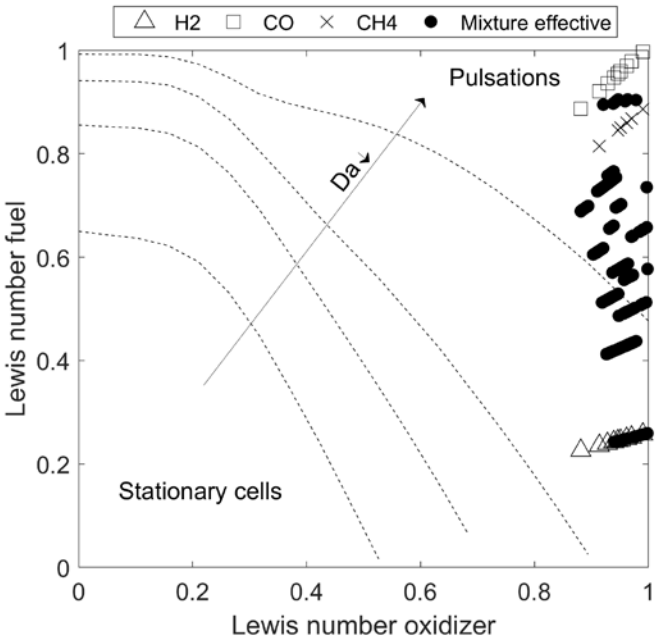

Figure 7: Stability map showing the Lewis numbers of the three fuel species and oxygen, as well as the effective Lewis number of the fuel mixture for the different flames studied in this paper. The instability zones are extracted from the theoretical findings of Cheatham and Matalon at $\phi = 1/3$ [31].

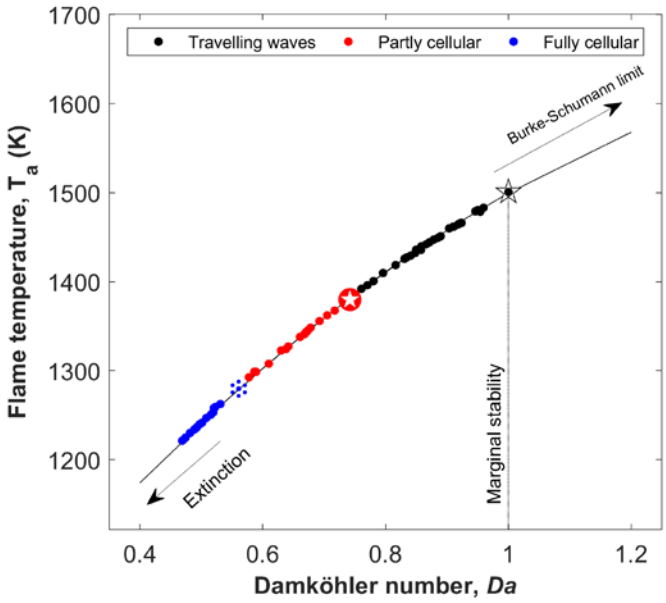

Figure 8: Top branch of the S-shaped response curve for the H_2-CO_2 flames. The shapes of unstable flames are indicated by symbols similar to those of Figure 6.

Linear stability analysis [31] has shown that the cell size (λ_c) for unstable single-fuel flames should scale as:

$$\lambda_c \sim (2\pi/\sigma^*) l_D \tag{3}$$

with σ^*being the non-dimensional preferred wavenumber at the instability onset and $l_D = D_{th}/U$ the diffusion length. σ^* is a function of U, ϕ, D_a, Le_o, and Le_F, and it can be determined numerically using the dispersion relation from stability analysis [12]. However, for the observed cellular H_2 flames, the value of σ^* seems to not vary significantly, as the measured λ_c values from the experiments scale almost linearly with l_D as shown in Figure 9. This was also reported in an earlier study using H_2 flames diluted with CO_2 in addition to helium [14].

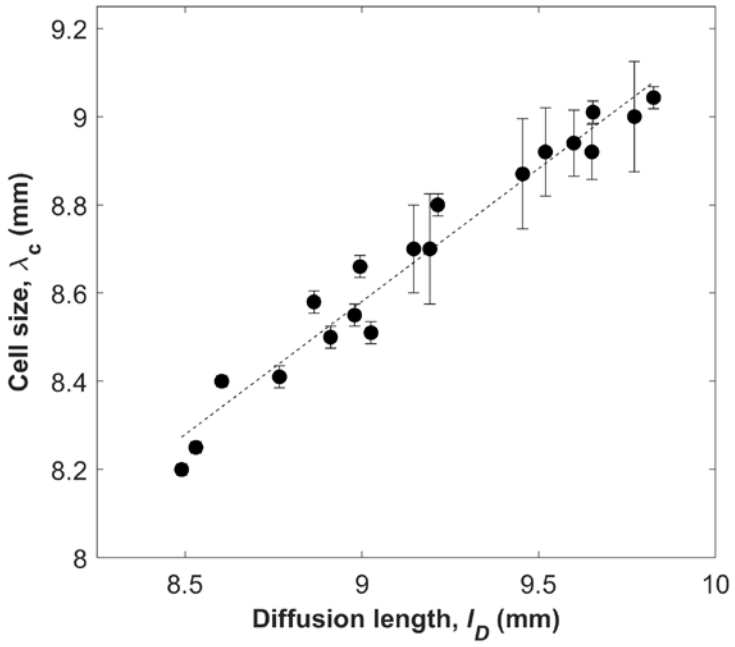

Figure 9: Measured cell size as a function of diffusion length for fully cellular H_2-CO_2 flames. The error bars represent uncertainty from the image analysis technique used.

3.2. CH_4-CO-CO_2 mixtures

Considering first CH_4-CO_2 mixtures without CO, and with $Le_{F,eff} = Le_{CH_4}$ approximately equal to 0.87, only planar intensity pulsations are observed in unstable flames. This is consistent with the theoretical instability map of Figure 7 and other investigations using CH_4 as a fuel [14]. Given that the average Lewis number of CO is 0.98 (Figure 7), one would expect a similar behavior for CO-rich fuel mixtures. This is confirmed over the broad range of CO-CH_4-CO_2 mixtures tested, as listed in Table 1, where the pulsation frequency and amplitude are reported. It should be noted that single-fuel CO-CO_2 mixtures are not investigated since these flames are not sustainable without the small addition of another hydrogen-containing species [32]. Linear stability analysis [33] shows that the pulsation frequency should scale as $f \sim (U^2/2\pi D_{th})\omega_I^*$, where ω_I^* is the oscillation frequency of the most unstable disturbance at marginal stability. An attempt to scale f with $U^2/2\pi D_{th}$ yielded scattered data for the flames presented, meaning that the value of ω_I^* significantly varies. Little has been discussed in theoretical work on the dependence of ω_I^* on the flame parameters such as D_a, ϕ, Le_F, and Le_o. However, as also reported in [14], we observe that for the CH_4-CO-CO_2 flames, the non-dimensional frequency scales linearly with Da as shown in Figure 10. Unlike cellular instabilities, pulsations are extremely sensitive to perturbations in

operating conditions, whereby their amplitude unsustainably increases and rapidly extinguishes the flame upon a very small decrease in fuel concentration or minute reduction in mixture strength.

Table 1: Parameters of the observed pulsating CH_4-CO-CO_2 flames.

Fuel	X_F (%)	ϕ	Le_o	$Le_{F,eff}$	Amplitude (%)	Frequency (hz)
100-0% CH4-CO	13	1.03	1.02	0.91	41	1.26
	12	1.09	1.01	0.91	32	1.18
75-25% CH4-CO	16	0.94	1.00	0.93	44	1.40
	15.5	0.94	1.00	0.92	20	1.39
	15	0.95	0.99	0.92	28	1.19
60-40% CH4-CO	16	0.88	0.97	0.91	38	1.19
	15	0.89	0.96	0.91	37	1.05
45-55% CH4-CO	17	0.81	0.95	0.91	33	1.05
	16.5	0.84	0.94	0.90	42	1.03
	16	0.88	0.94	0.90	34	0.95
30-70% CH4-CO	19	0.77	0.92	0.90	29	0.99
	18.5	0.83	0.92	0.92	30	0.90
	18	0.83	0.92	0.92	27	0.90

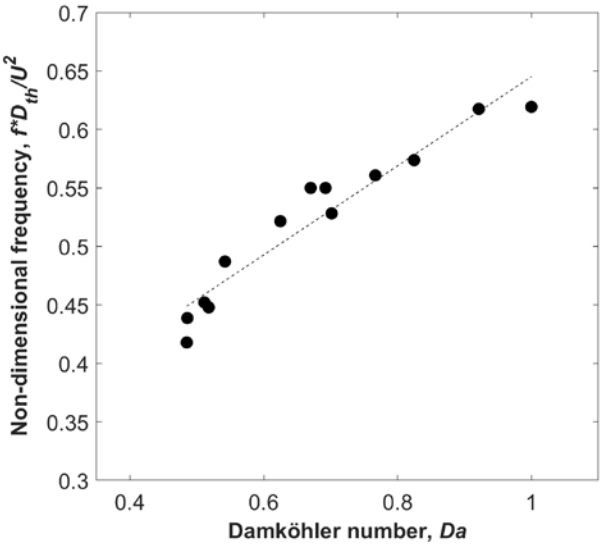

Figure 10: Non-dimensional pulsations frequency as a function of Damköhler number for unstable CH_4-CO mixtures.

3.3. H_2-CO-CO_2 mixtures

The addition of 25% pulsation-prone CO to H_2, which typically yields cellular instabilities, is considered. These mixtures yield $L_{F,eff}$ that is on average approximately 0.42, with their flame

stability limits shown in Figure 11. DTIs form within the shaded zone, and extinction is attained below and to the left-hand side of it. Only the instability type is shown, with its characteristics fully tabulated in the supplementary material. In the vicinity of the marginal stability state ($D_a = 1$ by assumption), when X_F = 23.5%, and down to X_F = 22.5%, only travelling waves are observed in $X_{H_2,CO} = 75\%$ flames. The number of waves is always four, exhibiting only rotational motion at frequencies varying between 3.1 and 3.4 Hz. Based on our earlier discussion with H_2-CO_2 flames, this is clearly caused by the H_2 in the mixture becoming unstable.

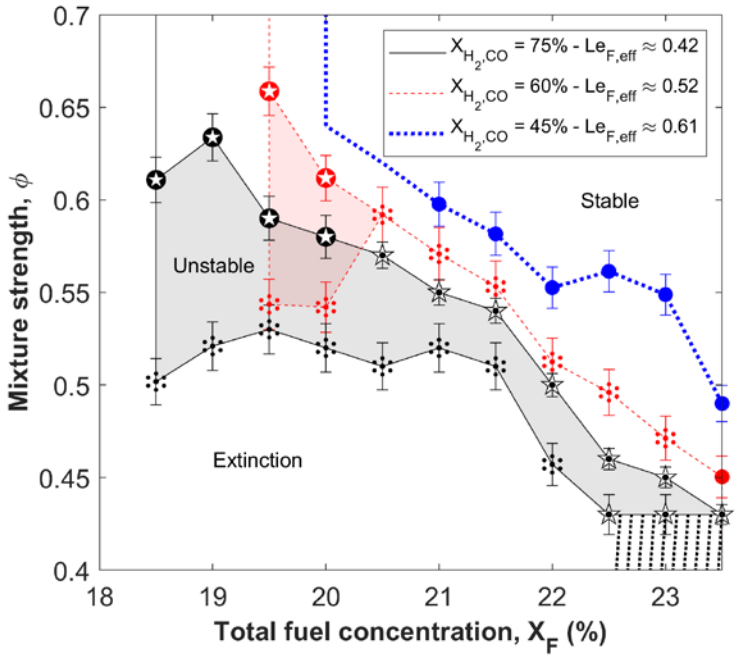

Figure 11: Flame stability limits for different H_2-CO binary fuels with no CH_4. The instability type is represented by symbols, and its characteristics are tabulated in the supplementary material. (●): Planar intensity pulsations, (✯): travelling waves, (✪): partly cellular, and (✣): fully cellular.

When D_a is reduced to 0.83 at $X_F = 22\%$, the consequences of adding CO to the fuel become visible as additional instabilities appear. Here, when the flame is perturbed, by for example slightly decreasing ϕ from 0.50 to 0.46 (0.25 SLPM increase in the oxidizer stream), flames with travelling waves start experiencing spatially-homogenous perturbations in their chemical reaction rate that are superimposed at 0.95 Hz, a frequency similar to that of the CO-rich fuels discussed in section 3.2. These grow after a few seconds into intense pulsations with a steady amplitude of approximately 57%, fragmenting and "prematurely" turning the flame fully cellular, as shown in Figure 12 and supplemental video #1.

After having taken over the travelling wave instabilities, the intensity pulsations of the now cellular flame result in axial oscillations spanning 28% of the combustion domain length. Such strong pulsations could never be sustained in any of the H_2-free flames, which suggest that CO may be extinct at the lowest intensity point of the instability cycle (Figure 12, position b). The H_2 appears to maintain the combustion process here, as the sizes of the four cells at this position scale linearly with the flame diffusion length, just as for the cells forming in single-fuel H_2 flames discussed in section 3.1. This is shown in Figure 13, where the cell sizes measured at the trough of the pulsation wave are presented for various multi-fuel flames. When the burning intensity of CO begins to increase, the cell sizes grow in-phase (Figure 12, position c-e) as the highest intensity point of the cycle is approached. Unlike for CH_4-CO fuels, the non-dimensional pulsation frequencies of H_2-containing flames do not scale linearly with the Damköhler number, whereby it is always lower than the linear scaling trend line. This is because the presence of H_2 in the fuel mixture temporarily dampens CO/CH_4 pulsations after the highest intensity point of the cycle, where the flame lingers around the mean position before the beginning of the next pulsation wave. This can be seen between positions e) and f) in the bottom plot of Figure 12, where the temporal variation in flame position is shown.

The pulsations intensity required to turn flames with travelling wave instabilities fully cellular decreases with decreasing D_a. This is because cellularity is inherently enhanced under these conditions, as was demonstrated earlier using H_2-CO_2 flames. The variation in the amplitude and frequency of different pulsation-induced cellular flames as a function of the Damköhler number is shown in the unshaded region of Figure 14. For the 75-25% H_2-CO case, the pulsations amplitude drops down to 8% at $Da = 0.69$. The periodic variation in the burning area exhibits a similar decrease, varying between 10-93% at $D_a = 0.83$, and only between 43-78% at $Da = 0.69$ (supplementary table). The cell spacing at the lowest intensity point of the cycle is also lowered from 20.1 mm to 14.9 mm as the number of cells increases.

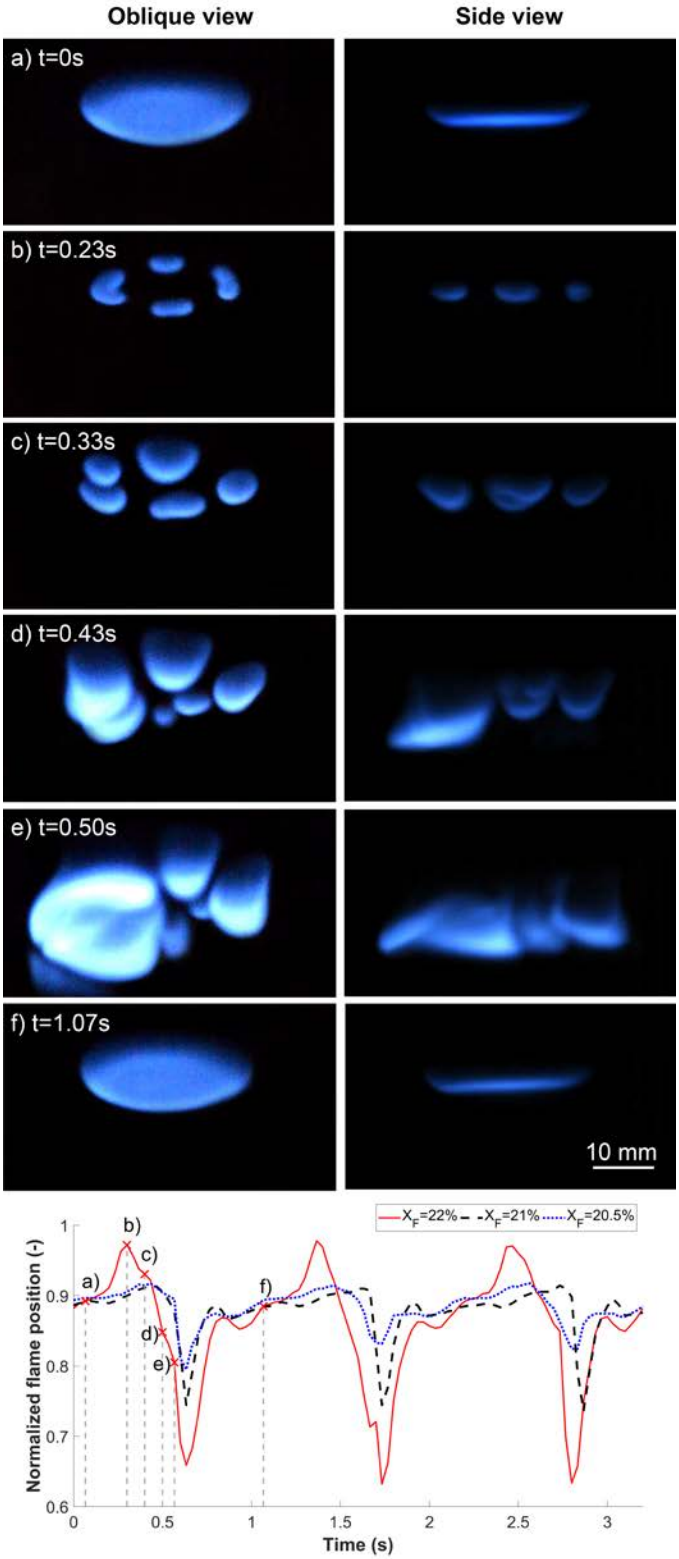

Figure 12: (a-f) Oblique and side views showing the instability cycle of a pulsation-induced cellular flame at X_F = 22%, ϕ = 0.46, $X_{H_2,CO}$ = 75%, and X_{CH_4} = 0%. (Video #1). Below, plot of the time variation in position of three such flames with different total fuel concentrations.

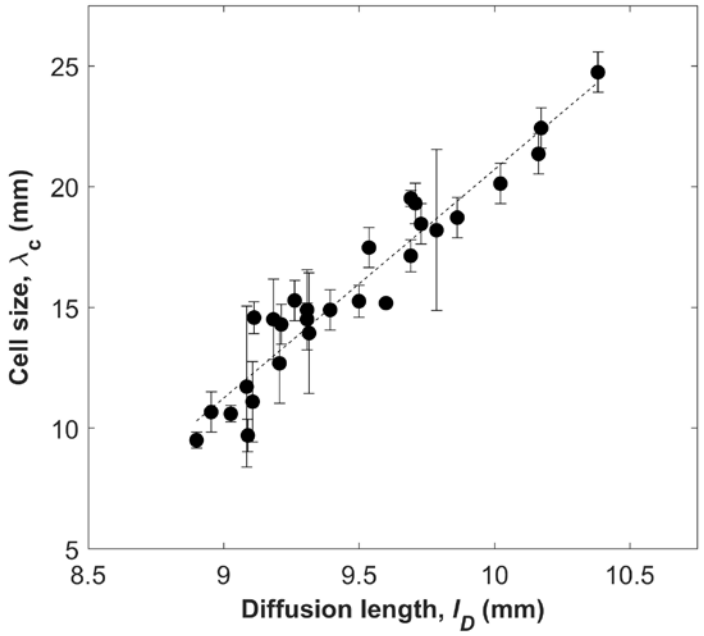

Figure 13: Cell size measured at the lowest intensity point of the pulsation cycle for the fully cellular multi-fuel flames. The error bars represent uncertainty from the image analysis technique used and from the simultanoues presence of intensity pulsations.

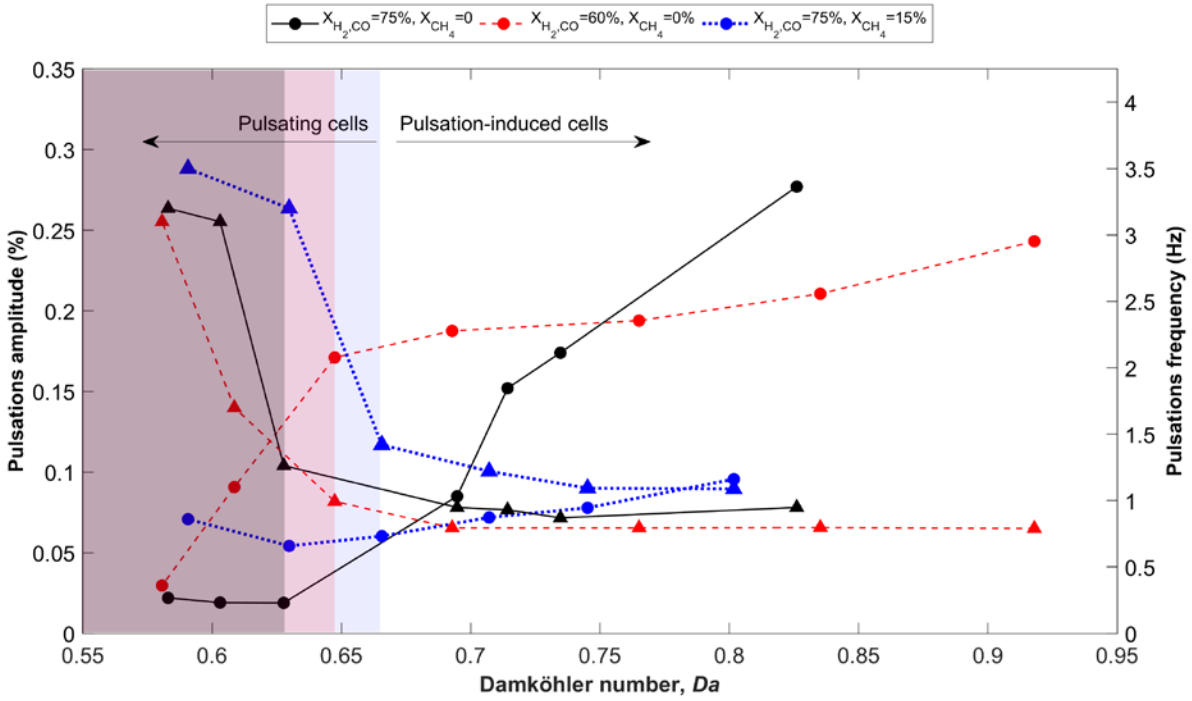

Figure 14: Variation in the amplitude (●) and frequency (▲) of the superimposed cellular-pulsations instabilities with Damköhler number. Pulsations amplitude is quantified in terms of the variation in flame position due to excessive cellularity.

Beyond a sufficiently small Damköhler number, intensity pulsations are no longer required to render flames with high fuel H_2 content fully cellular. This is because H_2-induced instabilities start manifesting themselves by the formation of stationary cells instead of travelling waves close to the lean extinction limit, as was also demonstrated earlier with H_2-CO_2 mixtures, and as observed with 75-25% H_2-CO flames in Figure 11 at $X_F = 18.5\%$ and $\phi = 0.61$. Now however, as CO perturbations onset, when ϕ is reduced to 0.5 in the latter case, the superimposed cellular-pulsation instabilities that develop have different characteristics compared to the pulsation-induced cellular flames that are formed at higher D_a. This is reflected by the abrupt trend change in the shaded region of Figure 14. When D_a is sufficiently low, the chemical reaction rate perturbations triggered by CO are manifested locally within each detached cell, instead of uniformly across a connected flame sheet, resulting in pulsations that are out-of-phase across a fragmented flame. The oscillations are now minimally dampened, with relatively fast frequencies exceeding 3 Hz, and with intensities that always grow unsustainably with time, leading to temporary extinction areas within the flame. The extinct cells are then replenished with ones undergoing earlier stages of the same pulsation cycle. This can be seen from supplemental video #2, where these pulsating cells are compared to the other mode with superimposed instabilities, pulsation-induced cells, which was discussed earlier in this section.

It is worth mentioning that the nature and mechanism of these superimposed DTIs in multi-fuel mixtures are different than the DTIs labelled as mixed in single-fuel flames. As discussed in section 3.1, the latter often refers to flames with cells rotating or periodically propagating along the flame sheet, and onset when the Lewis number of the only fuel species or oxidizer attains intermediate values. On the contrary, in mixtures such as syngas, the simultaneous presence of fuel species with distinctive Lewis numbers is what leads to superimposed instabilities, or cellular flames that experience pulsations in their chemical reaction rates. Unstrained diffusion flames are a convenient choice to demonstrate and study these intricate diffusive-thermal phenomena, which would otherwise be masked or rendered unsustainable by hydrodynamic effects, especially when it comes to intensity pulsations. As a result, studies in the literature addressing the stability of various multi-fuel flames often focus on hydrodynamics-driven cellular instabilities [34–36].

Figure 15 tracks the intensities of individual cells, from the moment they are formed and until they are extinguished, at 75-25% H_2-CO and different Damköhler numbers. It can be seen that the

number of cycles that can be sustained by each pulsating cell before extinction decreases with decreasing D_a. For $D_a = 0.63$, each cell undergoes approximately three pulsation cycles before it extinguishes. However, as D_a is lowered to 0.58, the number of pulses before local extinction approaches zero. Given that the actively burning area of the flame also drops, the cells generation rate filling these fastly-extinguishing zones, which is 3.2 Hz, becomes the limiting factor that determines the frequency of the superimposed instabilities near the lean extinction limit.

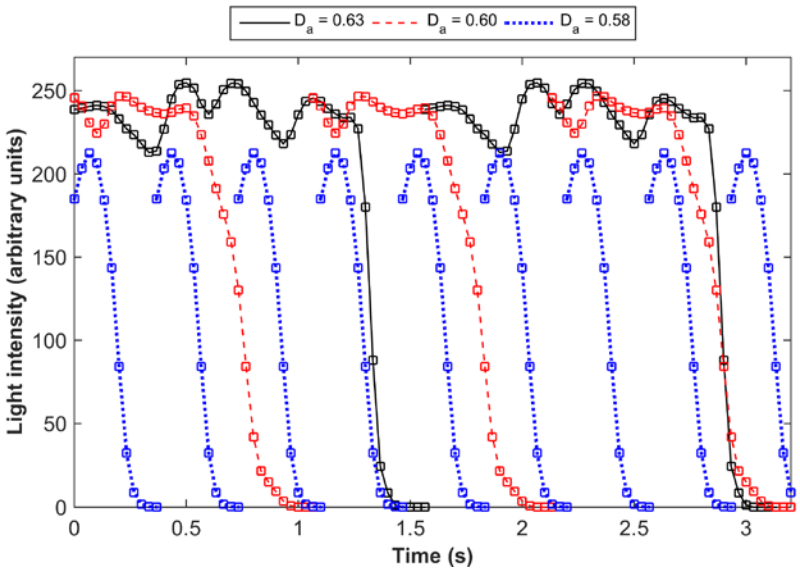

Figure 15: Light intensity emitted from pulsating cells at different Damköhler numbers in 75-25% H_2-CO mixtures. Each pulsation cycle represents a different cell before extinction.

The carbon monoxide content in the H_2-CO fuel mixture is now increased to $X_{H_2,CO} = 60\%$, yielding a fuel Lewis number of $Le_{F,eff} = 0.52$ on average. From the resulting stability limits shown in Figure 11, it can be seen that this significantly reduces the operating range where sustainable DTIs form, which in fact shrinks into a line at $X_F \geq 20.5\%$. This is because CO becomes unstable before H_2 in this mixture, as sensitive planar intensity pulsations are observed at the marginal stability state instead of travelling waves. At lower Damköhler numbers, 1-Hz pulsation-induced cells form, since the inherent enhancement in cellularity of H_2 means that lower-amplitude perturbations, 24% in this case, are now required to render the flame fully cellular. Here again, the pulsations amplitudes keep decreasing with D_a, reaching 17% at $D_a = 0.65$ as shown in Figure 14. Beyond this point, H_2 cells begin preceding CO pulsations, and the instability zone regains its broadness (Figure 11). This represents the inherent cellularity tipping point discussed

in the previous paragraph, where cellular flames exhibiting fast pulsations at approximately 3 Hz are formed.

As the CO content in the fuel exceeds that of H_2 at $X_{H_2,CO}$ = 45% with $Le_{F,eff}$ being approximately 0.61, the whole flame stability zone shrinks to a line below and to the left of which the flame is extinct (Figure 11). Cells are never observed in unstable flames, which exhibit only planar intensity pulsations, indicated by solid circles in Figure 11. The pulsation frequencies vary between 0.8 and 1.0 Hz (supplementary table). The amplitude of pulsations that can be sustained decreases as D_a is lowered by decreasing the fuel concentration, going from 53% at $X_F = 24\%$ to 7% at $X_F = 21\%$. Beyond this point, the pulsations that onset are never steady and their intensities rapidly grow, causing the flame to extinguish within a few seconds.

3.4. H_2-CO-CH_4-CO_2 mixtures

The addition of different amounts of CH_4 to $X_{H_2,CO} = 75\%$ mixtures is now considered, with the flame stability limits shown in Figure 16. For the X_{CH_4} = 15% case, which yields $Le_{F,eff}$ around 0.50, CH_4/CO-induced instabilities onset before those caused by H_2, as planar intensity pulsations are observed close to the marginal stability state. At lower Damköhler numbers, pulsation-induced cells form, and their amplitudes drop from 10% at $D_a = 0.8$ to 6% at $D_a = 0.67$, below which the inherent cellularity tipping point is crossed as can be seen from Figure 14.

When the CH_4 in the fuel is increased to X_{CH_4} = 30% ($Le_{F,eff} \approx 0.6$), cells never form at any D_a. At the marginal stability state, occurring when X_F = 17%, planar intensity pulsations onset with an amplitude and frequency of 22% and 1.0 Hz, respectively. These persist when X_F is decreased to 16.5%, albeit with a lower amplitude of 16%. At even lower D_a, the pulsations that onset are always unsustainable, as the flame is forced during part of the pulsation cycle into the highly oxygenated injection layer in the burner where the flow is three-dimensional.

Comparing the addition of CH_4 to that of CO through Figure 11 and Figure 16, a clear resemblance is observed, highlighting the importance of the effective fuel Lewis number in predicting the type of instabilities formed. In both of these flame stability maps, when $Le_{F,eff}$ is approximately 0.5, the instability zone shrinks after the marginal stability state, as planar intensity pulsations onset followed by pulsation-induced cells. As the lean extinction limit is approached, the instability zone broadens as inherently cellular flames are formed. Similarly, when $Le_{F,eff}$

exceeds 0.6, only planar intensity pulsations are observed in unstable flames, irrespective of whether CO or CH_4 is added.

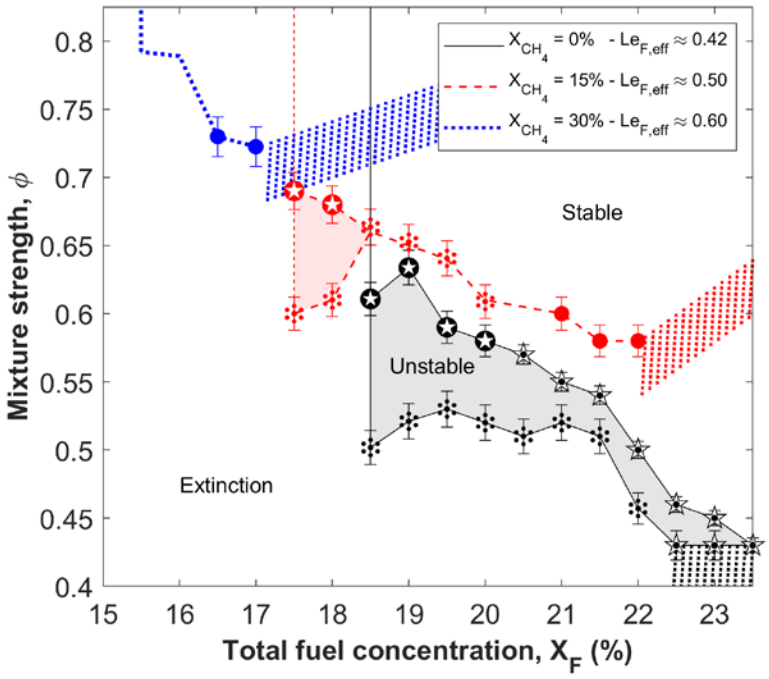

Figure 16: Effect of CH_4 addition on the flame stability limits at $X_{H_2,CO} = 75\%$. The symbols indicate the type of instability, with its characteristics provided in the supplementary material. (●): Planar intensity pulsations, (✯): travelling waves, (✪): partly cellular, and (✣): fully cellular. Hatched regions represent conditions that are not tested.

In fact, if CH_4 completely replaces CO in quantities such that the same $Le_{F,eff}$ is maintained, the same instability types and sequence are always observed. This was confirmed by the flame stability limits produced using a broad range of H_2-CH_4 mixtures. Consequently, a generalized qualitative DTI map is proposed in Figure 17, in terms of the effective fuel mixture Lewis number and the flame Damköhler number. Using these two fundamental parameters, the various degrees of cellularity and intensity pulsations that can simultaneously form in lean dry syngas flames can be predicted. The map reveals that when $Le_{F,eff}$ is lower than 0.25, unstable flames never exhibit intensity pulsations. Nonetheless, these flames can exhibit various degrees of cellularity going from travelling waves at marginal stability to stationary cells near the extinction limit. For $Le_{F,eff}$ around 0.4, pulsations can onset simultaneously with cells, and this can lead to pulsation-induced cells at high D_a or pulsating cells near the extinction limit, as detailed in section 3.3. At $Le_{F,eff}$ of

approximately 0.5, purely cellular flames no longer form, and unstable flames always exhibit pulsations in their chemical reaction rates. Finally, when $Le_{F,eff}$ exceeds 0.6, flame cellularity is diminished and only planar intensity pulsations onset.

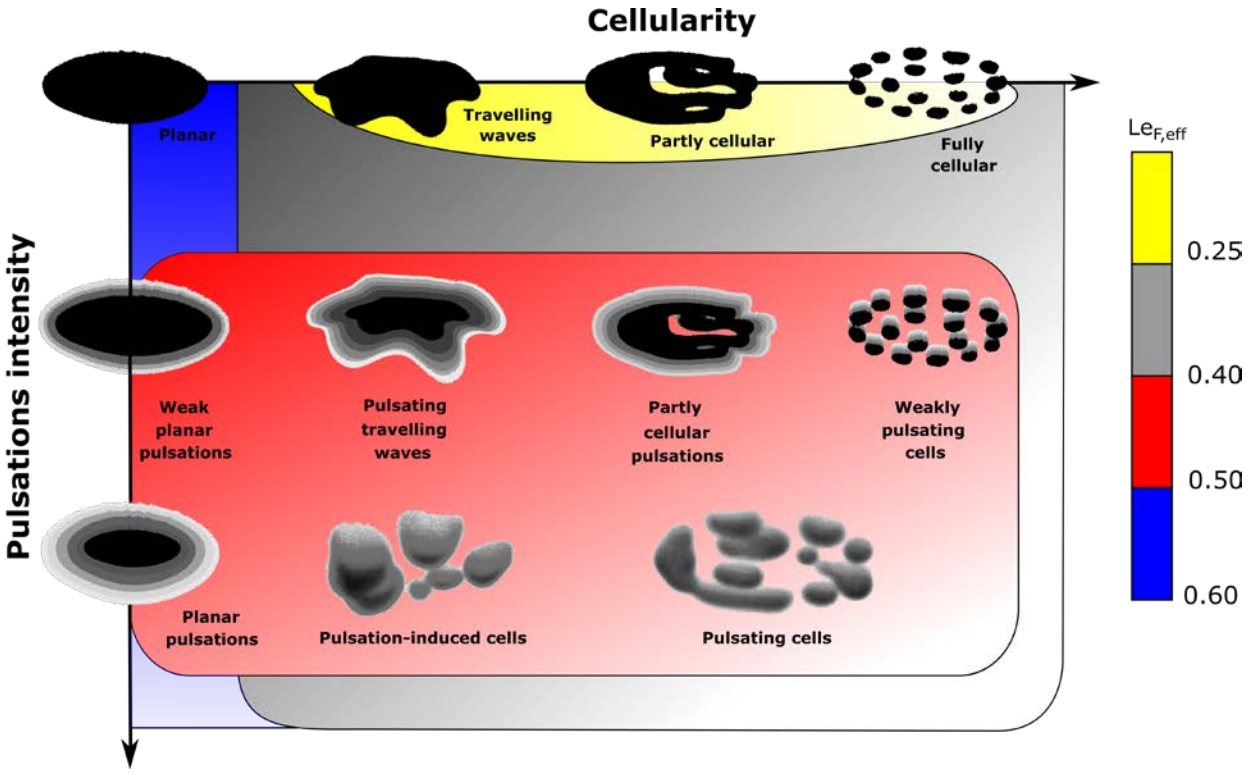

Figure 17: Qualitative illustration of the instabilities that onset in unstrained syngas diffusion flames with various fuel mixture Lewis numbers and $Le_o \approx 0.97$. The Damköhler number is represented by the relative shading level, where dark = near marginal stability, and light = near extinction.

Evidently, owing to the different combustion chemistry of each fuel species, the flammability limits of different fuel mixtures remain unique even if their $Le_{F,eff}$ is the same. To complete the discussion, the flammability limits for $X_{H_2,CO} = \{30\%, 45\%, 60\%, 75\%\}$ and $X_{CH_4} = \{0\%, 15\%, 30\%\}$ are presented in Figure 18. Looking at the effect of the H_2/CO ratio, it can be seen that lower fuel concentrations and mixture strengths are required for instabilities to onset at higher H_2 content. Since these conditions result in lower burning intensities, H_2-rich unstrained syngas flames are deemed more stable than CO-rich blends. For instance, increasing the relative H_2 amount from $X_{H_2,CO} = 30\%$ to 75% results in delaying the onset of DTIs from $X_F = 25\%$ to 23.5% in fuels without CH_4, and from $X_F = 24\%$ to 20% when $X_{CH_4} = 15\%$ is added. The same conclusion is drawn from the dilution-induced extinction limits, beyond which no flame can be

established within the one-dimensional combustion zone at any mixture strength. When the relative amount of H_2 to CO is increased from $X_{H_2,CO} = 30\%$ to 75% at $X_{CH_4} = 0\%$, extinction is delayed from $X_F = 20\%$ to 18.5%, and from $X_F = 18.5\%$ to 17.5% at $X_{CH_4} = 15\%$. This also demonstrates that flammability is substantially enhanced upon the addition of CH_4 to syngas. For example, at $X_{H_2,CO} = 45\%$, extinction is delayed from $X_F = 20\%$ to 18.5% when 15% CH_4 is added to syngas, and down to $X_F = 16\%$ at $X_{CH_4} = 30\%$.

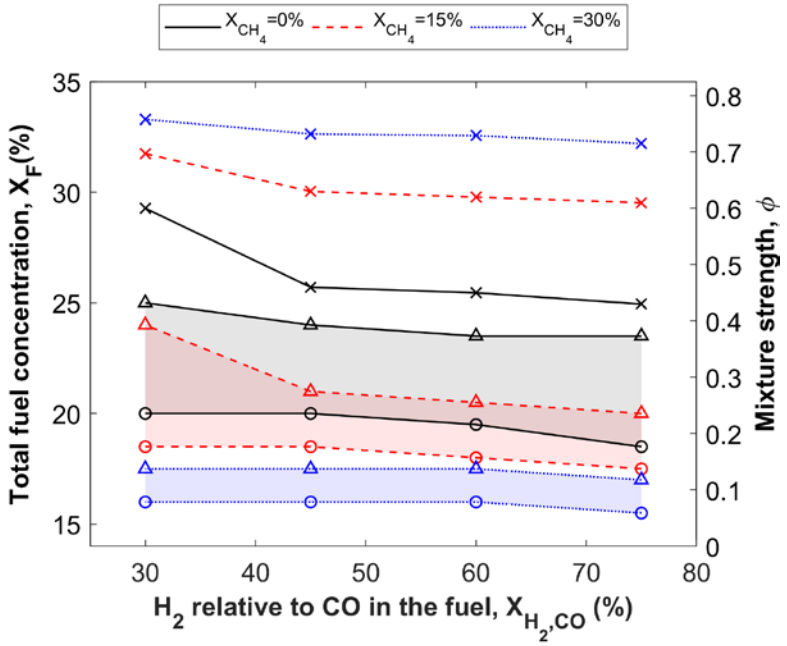

Figure 18: Flammability limits for different syngas compositions. The first onset of instabilities is indicated by (△), and CO_2 dilution–induced extinction is represented by (○). Onset of instabilities in terms of mixture strength is also given by (x).

4. Conclusion

Unstrained diffusion flames of multi-fuel mixtures are experimentally characterized for the first time in this paper. Understanding of the diffusive-thermal instabilities that onset in lean biomass-derived syngas mixtures is provided, whose efficient combustion plays a crucial role in the overall efficiency of biorefinaries. With $Le_o \approx 0.97$ as imposed by the abundant CO_2 species, it is shown that H_2 with $Le_{H_2} \approx 0.25$ promotes travelling waves in the flame at the marginal stability state, and stationary cellular instabilities at lower Damköhler numbers. On the other hand, CH_4 with $Le_{CH_4} \approx 0.88$ and CO with $Le_{CO} \approx 0.98$ both always induce chemical reaction rate pulsations. After determining the flame stability limits for a broad range of H_2+CO+CH_4+CO_2

mixtures, the different instability patterns are clearly seen to compete and interact with each other, leading to superimposed DTI modes with various degrees of cellularity and pulsation, depending on an effective mixture-averaged Lewis number of the fuel and on the Damköhler number.

For H_2-CO-CH_4 fuels with $Le_{F,eff} \geq 0.6$, only planar intensity pulsations with no cellular instabilities form for all Damköhler numbers beyond the marginal stability state. However, when the fuel mixture contains relatively low amounts of CO/CH_4, such that $0.25 < Le_{F,eff} \leq 0.5$, intense CO/$CH_4$-induced chemical reaction rate pulsations with an amplitude reaching 57% turn the planar flame front fully cellular. These pulsation-induced cells vary in number between four and eight, as they oscillate in-phase at a CO/CH_4-dominated frequency of approximately 1 Hz. The amplitude of pulsations required to turn H_2-rich fuel blends "prematurely" fully cellular decreases with Damköhler number, and the flame front becomes inherently cellular under sufficiently weakly burning conditions. Now, when the CO/CH_4 perturbations onset, they develop into out-of-phase pulsations across the fragmented flame sheet, with relatively large frequencies that exceed 3 Hz. These superimposed fast pulsations grow unsustainably with time leading to local extinction spots, which are then occupied by other younger pulsating cells. The number of pulses that can be sustained by each cell before extinction and the actively burning area drastically drop as the lean extinction limit is approached, leading to superimposed instabilities with frequencies now dominated by the H_2 cells generation rate, which is approximately 3.2 Hz.

High-speed imaging of the observed superimposed cellular-pulsation instabilities reveals that the cell sizes at the lowest intensity point of the pulsation cycle, where CO/CH_4 burns the weakest, scale linearly with diffusion length. A similar scaling behaviour is observed for the sizes of the cells forming in single-fuel H_2 flames, signalling that CO and CH_4 may be temporarily extinct at the trough of the pulsation cycle, and that the H_2 in the fuel mixture contributes to sustaining these intense pulsations. Extracting the Fourier transforms of the pulsation cycles show that H_2 dampens the CO/CH_4 oscillations, especially when far from the lean extinction limit, as the reduced non-dimensional frequency does not scale with Damköhler number, unlike for CH_4-CO flames.

Acknowledgements

The authors are grateful for the funders of this work: The Trottier Energy Institute (Trottier scholarship and project grant), and the Natural Sciences and Engineering Research Council of

Canada (NSERC) through the postgraduate doctoral scholarship (PGSD3 - 546588 – 2020), and discovery grants (RGPIN-03622-2014 and RGPIN-05071-2022).

Supplementary material

Two videos and supplementary figures are provided, along with a table that includes the characteristics of the unstable flames in Figure 11 and Figure 16.

Nomenclature

$\mathfrak{B}$: Arrhenius pre-exponential factor (m^3/mol s)

c_p: Specific heat at constant pressure (J/kg K)

Da: Damköhler number (-)

D_i: Diffusivity of species i (m^2/s)

D_{th}: Thermal diffusivity (m^2/s)

DTI: Diffusive-thermal instability

E: Activation energy (J/mol)

f: Pulsation frequency (1/s)

l_D: Diffusion length (m)

L: Length of the one-dimensional combustion zone (m)

Le_i: Lewis number of species i

$Le_{F,eff}$: Effective fuel Lewis number

p_0: Ambient pressure (Pa)

q: Heat release per unit mass of fuel (J/kg)

R: Ideal gas constant (J/kg mol)

T_a: Adiabatic flame temperature (K)

T_L: Temperature at the top of the one-dimensional combustion zone (K)

U: Bulk velocity (m/s)

$\overline{W}$: Mean molecular weight (kg/kmol)

W_i: Molecular weight of species i (kg/kmol)

x_f: Normalized flame position (-)

X_i: Molar fraction of species $i = \{H_2, CO, CH_4\}$ relative to the other combustible species in the fuel stream (-)

$X_{H_2,CO}$: Molar fraction of H_2 relative to CO in the fuel stream (-)

X_F: Total fuel concentration (-)

Y_i: Mass fraction of species i (-)

λ: Thermal conductivity (W/m K)

λ_c: Cell size (mm)

ν_i: Stoichiometric coefficient of species i

ϕ: Mixture strength (-)

ρ: Density (kg/m^3)

ΔT: Temperature difference between top and bottom of the 1D combustion zone (K)

References

[1] L. Jiang, C. Gu, G. Zhou, F. Li, Q. Wang, Cellular instabilities of n-butane/air flat flames probing by PLIF-OH and PLIF-CH2O laser diagnosis, Exp. Therm. Fluid Sci. 118 (2020).

[2] T. Poinsot, Prediction and control of combustion instabilities in real engines, Proc. Combust. Inst. 36 (2017) 1–28.

[3] M. Matalon, Flame dynamics, Proc. Combust. Inst. 32 I (2009) 57–82.

[4] D. Lo Jacono, P.A. Monkewitz, Scaling of cell size in cellular instabilities of nonpremixed jet flames, Combust. Flame. 151 (2007) 321–332.

[5] M. Füri, P. Papas, P.A. Monkewitz, Non-premixed jet flame pulsations near extinction, Proc. Combust. Inst. 28 (2000) 831–838.

[6] M. Matalon, Intrinsic Flame Instabilities in Premixed and Nonpremixed Combustion, Annu. Rev. Fluid Mech. 39 (2007) 163–191.

[7] L.. Kirkby, R.A. Schmitz, An Analytical Study of the Stability of a Laminar Diffusion Flame, Combust. Flame. 10 (1966) 205–220.

[8] E. Robert, P.A. Monkewitz, Experiments in a novel quasi-ID diffusion flame with variable bulk flow, Proc. Combust. Inst. 32 I (2009) 987–994.

[9] J. Buckmaster, A. Nachman, S. Taliaferro, The fast-time instability of diffusion flames, Phys. D Nonlinear Phenom. 9 (1983) 408–424.

[10] J.S. Kim, F.A. Williams, Extinction of diffusion flames with nonunity Lewis numbers, J. Eng. Math. 1997 312. 31 (1997) 101–118.

[11] M. Matalon, G.S.S. Ludford, J. Buckmaster, Diffusion flames in a chamber, Acta Astronaut. 6 (1979) 943–959.

[12] P. Metzener, M. Matalon, Diffusive-thermal instabilities of diffusion flames: onset of cells and oscillations, Combust. Theory Model. 10 (2006) 701–725.

[13] E. Robert, P.A. Monkewitz, Experimental realization and characterization of unstretched planar one-dimensional diffusion flames, Combust. Flame. 160 (2013) 546–556.

[14] E. Robert, P.A. Monkewitz, Thermal-diffusive instabilities in unstretched, planar diffusion flames, Combust. Flame. 159 (2012) 1228–1238.

[15] A. Molino, S. Chianese, D. Musmarra, Biomass gasification technology: The state of the art overview, J. Energy Chem. 25 (2016) 10–25.

[16] E. Antar, E. Robert, Thermodynamic analysis of novel methanol polygeneration systems for greenhouses, Biomass Convers. Biorefinery. (2021).

[17] O. Askari, Z. Wang, K. Vien, M. Sirio, H. Metghalchi, On the flame stability and laminar burning speeds of syngas/O2/He premixed flame, Fuel. 190 (2017) 90–103.

[18] Z. Wang, Z. Bai, G. Yu, S. Yelishala, H. Metghalchi, The Critical Pressure at the Onset of Flame Instability of Syngas/Air/Diluent Outwardly Expanding Flame at Different Initial Temperatures and Pressures, J. Energy Resour. Technol. 141 (2019).

[19] R.W. Francisco, A.A.M. Oliveira, Measurement of the adiabatic flame speed and overall activation energy of a methane enriched H2/CO/CO2/N2 low heating value mixture, Int. J. Hydrogen Energy. 45 (2020) 29533–29545.

[20] W. Jin, J. Wang, S. Yu, Y. Nie, Y. Xie, Z. Huang, Cellular instabilities of non-adiabatic laminar flat methane/hydrogen oxy-fuel flames highly diluted with CO2, Fuel. 143 (2015) 38–46.

[21] J. Natarajan, T. Lieuwen, J. Seitzman, Laminar flame speeds of H2/CO mixtures: Effect of CO2 dilution, preheat temperature, and pressure, Combust. Flame. 151 (2007) 104–119.

[22] H.A. Yepes, A.A. Amell, Laminar burning velocity with oxygen-enriched air of syngas produced from biomass gasification, Int. J. Hydrogen Energy. 38 (2013) 7519–7527.

[23] É. Robert, Experimental Investigation of Unstrained Diffusion Flames and their Instabilities, PhD thesis, Ecole Polytechnique Federale de Lausanne, 2008.

[24] E. Robert, Mass spectrometer calibration over wide concentration ranges in multicomponent gas mixtures, Meas. Sci. Technol. 21 (2010).

[25] D. Lo Jacono, P. Papas, M. Matalon, P.A. Monkewitz, An experimental realization of an unstrained, planar diffusion flame, Proc. Combust. Inst. 30 (2005) 501–509.

[26] D.G. Goodwin, R.L. Speth, H.K. Moffat, B.W. Weber, Cantera: An Object-oriented Software Toolkit for Chemical Kinetics, Thermodynamics, and Transport Processes, (2021).

[27] R.J. Kee, M.E. Coltrin, P. Glarborg, Chemically Reacting Flow: Theory and Practice, John Wiley & Sons, 2003.

[28] E. Bodenschatz, W. Pesch, G. Ahlers, Recent Developments in Rayleigh-Bénard Convection, Annu. Rev. Fluid Mech. 32 (2000) 709–778.

[29] S. Hu, R.W. Pitz, Y. Wang, Extinction and near-extinction instability of non-premixed

tubular flames, Combust. Flame. 156 (2009) 90–98.

[30] S.W. Shopoff, P. Wang, R.W. Pitz, Experimental study of cellular instability and extinction of non-premixed opposed-flow tubular flames, Combust. Flame. 158 (2011) 2165–2177.

[31] S. Cheatham, M. Matalon, A general asymptotic theory of diffusion flames with application to cellular instability, J. Fluid Mech. 414 (2000) 105–144.

[32] H.-Y. Shih, J.-R. Hsu, Y.-H. Lin, Computed flammability limits of opposed-jet H2/CO syngas diffusion flames, Int. J. Hydrogen Energy. 39 (2014) 3459–3468.

[33] S. Kukuck, & M. Matalon, The onset of oscillations in diffusion flames, Combust. Theory Model. 5 (2001) 217–240.

[34] H. Lulic, A. Breicher, A. Scholtissek, P.E. Lapenna, A. Dreizler, F. Creta, C. Hasse, D. Geyer, F. Ferraro, On polyhedral structures of lean methane/hydrogen Bunsen flames: Combined experimental and numerical analysis, Proc. Combust. Inst. (2022).

[35] E.C. Okafor, Y. Nagano, T. Kitagawa, Experimental and theoretical analysis of cellular instability in lean H2-CH4-air flames at elevated pressures, Int. J. Hydrogen Energy. 41 (2016) 6581–6592.

[36] T. Piemsinlapakunchon, M.C. Paul, Effect of syngas fuel compositions on the occurrence of instability of laminar diffusion flame, Int. J. Hydrogen Energy. 46 (2021) 7573–7588.